Charge transport of the mesoscopic metallic state in partially crystalline polyanilines

J. Joo
Department of Physics, The Ohio State University, Columbus, Ohio 43210-1106
and Department of Physics, Korea University, Seoul 136-701, Korea

S. M. Long
Department of Physics, The Ohio State University, Columbus, Ohio 43210-1106

J. P. Pouget
Laboratoire de Physique des Solides, CNRS URA 02, Université Paris-Sud, 91405 Orsay, France

E. J. Oh* and A. G. MacDiarmid
Department of Chemistry, University of Pennsylvania, Philadelphia, Pennsylvania 19104-6323

A. J. Epstein
Department of Physics and Department of Chemistry, The Ohio State University, Columbus, Ohio 43210-1106
(Received 21 March 1997; revised manuscript received 18 November 1997)

Charge transport properties, including temperature-dependent dc conductivity, thermoelectric power, electron paramagnetic resonance, microwave frequency dielectric constant and conductivity, and electric-field-dependent conductance of partially crystalline (''physically'' cross-linked) HCl-doped polyaniline correlated with x-ray structure studies, demonstrate that charge delocalization in physically cross-linked polyaniline systems is structurally controlled. Further, we observe a positive dielectric constant at room temperature which increases (to values $\geqslant 10^4$) with increasing percent crystallinity, the size of crystalline regions, and polymer chain alignment in the disordered regions, supporting the establishment of mesoscopic metallic regions. We propose an inhomogeneous disorder model for this system in which ordered (crystalline) regions, described by three-dimensional metallic states, are connected through amorphous regions of polymer chains where one-dimensional disorder-induced localization is dominant. We utilize the metallic box, interrupted metallic strands, and Nakhmedov's phonon-induced delocalization models to account for the temperature dependence of charge transport properties of the various partially crystalline polyanilines. Analyses for the sample and temperature-dependent electron paramagnetic resonance linewidth and thermoelectric power are presented. [S0163-1829(98)04515-9]

I. INTRODUCTION

Conducting polymers such as doped polyacetylene, polyaniline, and polypyrrole have generated considerable interest in fundamental and applied research after the first report of doped polyacetylene in 1977.[1,2] Mobile charged defects (solitons, polarons, and bipolarons) in lightly doped one-dimensional chains,[3–9] and disorder-induced charge localization in heavily doped systems,[10–16] have attracted much attention. Transport models for three-dimensional amorphous semiconductors[17] often have been used to account for the charge delocalization phenomena in conducting polymers, despite fundamental differences. In conducting polymers the dopant ions are positioned interstitially between chains, where as in conventional semiconductors they are usually substituted directly into the host lattice. Further, covalent bonding along polymer chains, and weak bonding between them result in a quasi-one-dimensional morphology which has important roles in the charge delocalization of these systems.[18–23] In almost all cases, the conductivities of these materials decrease with decreasing temperature unlike conventional metals, even though their conductivities at room temperature may be as high as $\sim 10^4$ S cm^{-1}.

A common goal in charge transport studies of conducting polymers is the determination of the nature of the intrinsic metallic state, where conductivities (σ) at room temperature comparable to standard metals ($\sigma_{dc} \sim 10^4 - 10^5$ S cm^{-1}) and negative $d\sigma/dT$ (T is the temperature) have been observed. However, there have been many controversial issues concerning the absolute conductivities and details of the charge transport mechanisms. A central issue is whether the metallic states are predominately one dimensional (1D) (Ref. 24) or three dimensional (3D).[15,25] For example, the 1D random dimer model using resonance tunneling has been proposed to explain the charge delocalization.[24] On the other hand, both theoretical[18,26–28] and experimental[15,25,29–31] studies have emerged emphasizing the importance of interchain interaction. A second controversy is whether the origin of the localization phenomena is passage of 1D chains through disordered regions (based on the inhomogeneous disorder model) (Refs. 19, 20, 22, 25, and 30) or 3D homogeneous disorder.[12,31] A third controversy is whether charge transport is due to variable range hopping (VRH) (Refs. 15 and 29), with emphasis on interchain hopping in disordered regions or charge energy limited tunneling based on the granular metallic model (GMM).[11,32,33] The quasi-1D VRH model empha-

sizes nearest-neighbor interchain hopping in disordered regions, while the GMM uses charge tunneling between metallic islands. The fundamental assumption of the GMM is that the metallic islands are embedded in an insulating background, and that there is distinct phase segregation between the two states. All of these controversial issues originate from the complex morphology associated with conducting polymers.

The highly conducting state of the emeraldine salt form of polyaniline (PAN-ES) doped with hydrochloric acid (HCl) has been intensively studied for the past decade.[2,11–13,15,19,21,24,25,29–40] PAN-ES is obtained by addition of protons to the insulating emeraldine base form of polyaniline (EB) through treatment with acid. Thus there is no addition or removal of electrons to form the conducting state.[35] With the recent advances in chemical processing the crystallinity and intrinsic transport properties, such as conductivity, have been improved. For example, the dc conductivity of HCl-doped PAN-ES was reported to be ~ 0.1 in 1986,[34] ~ 1 in 1989,[36] ~ 20 in 1991,[15] and in excess of 100 S cm^{-1} in 1993.[38] Recently, σ_{dc} of camphor-sulfonic-acid-doped polyaniline processed from *m*-cresol solvent [PAN-CSA (*m*-cresol)] was reported to be ~ 400 S cm^{-1} at room temperature.[19,39] The microwave dielectric constant (ϵ_{mw}) and its temperature dependence changed dramatically as the quality of polyaniline materials was improved.[15,19,25,36] For example, at room temperature the values of ϵ_{mw} increased from ~ 10 to ~ 100 to $\sim 40\,000$ then decreased to $\sim -80\,000$ as the conductivity increased from ~ 0.1 to ~ 1 to ~ 100 to ~ 400 S cm^{-1}, respectively.

In this paper, we apply the experimental methods of x-ray diffraction, charge transport, and electron paramagnetic resonance (EPR) to study charge delocalization in partially crystalline HCl-doped PAN-ES samples with differing degrees of crystallinity. The quasi-1D VRH model,[15,29] applied to charge transport in the disordered regions is shown to account for the temperature-dependent dc conductivity, thermoelectric power, and high-electric-field-dependent conductance. Also, from the correlation between the low-temperature microwave dielectric constant and the crystalline coherence lengths obtained from x-ray diffraction, a 3D metallic state is identified. Transport results show that the scale of charge delocalization in the highest crystalline materials is mesoscopic rather than microscopic. It is demonstrated that the charge delocalization is structurally controlled.

In Sec. II of this paper, the charge transport properties of quasi-1D disordered systems are reviewed. Also in Sec. II, the metallic box, interrupted metallic strands, and the model of Nakhmedov, Prigodin, and Samukhin are introduced, which later are used to account for the temperature dependence of the microwave dielectric constant and the conductivity of polyaniline with various degrees of crystallinity. The experimental principles and techniques for x-ray diffraction, charge transport, and EPR are described in Sec. III. The materials and experimental results are presented in Sec. IV, followed by a discussion in Sec. V. Finally, we summarize this study in Sec. VI.

II. THEORETICAL BACKGROUND

A. Charge transport properties of quasi-1D disordered systems

The quasi-1D VRH model emphasizing nearest-neighbor interchain hopping has been used to account for the macroscopic dc charge transport of polyanilines.[15] For this model,

$$\sigma_{dc} \propto \exp\left[-\left(\frac{T_0}{T}\right)^{1/2}\right], \tag{1}$$

where $T_0 = 16/(k_B N(E_F) L_\parallel L_\perp^2)$, $N(E_F)$ is the density of states at the Fermi level, and $L_\parallel (L_\perp)$ is the localization length in the parallel (perpendicular) direction.[15,25,29] T_0 can be interpreted as an effective energy barrier between localized states, and is a measurement of the degree of disorder in disordered regions. For example, polyaniline samples with relatively larger T_0 have greater disorder in the disordered regions, where the charge cannot effectively delocalize. The granular metallic model of Sheng, incorporating charging-energy-limited tunneling, predicts the same temperature dependence of dc conductivity, i.e., $\sigma_{dc} \propto \exp[-(T_0/T)^{1/2}]$.[32,33]

The generalized formula for the electric-field-dependent conductivity $[\sigma(E)]$ for disordered systems in low electric fields [E is approximately less than or equal to 10^3 V cm^{-1} (Ref. 17)] is $\sigma(E) \propto \exp(eRE/k_BT)$, where R is the most probable hopping distance. However, $\sigma(E)$ at high electric fields [$E \gg E_t \equiv k_BT/(eR)$; i.e., the energy gained by an electron in the electric field, eRE, is larger than the average hopping energy, allowing the electron to move by hopping to lower E while emitting a phonon[17]] can distinguish quasi-1D VRH and tunneling. When the applied E field significantly exceeds the threshold field E_t, $\sigma(E)$ is described by

$$\sigma(E) = \sigma_0 \exp\left[\left(\frac{E}{E_0}\right)^{1/(d+1)}\right], \tag{2}$$

where $d = 0$, 1, and 3 correspond to the GMM,[32,33] the quasi-1D VRH model,[29] and the 3D VRH model,[17] respectively, and E_0 is a constant.

There are several theories for the thermoelectric power (S) of inhomogeneous media. For example, effective-medium and percolation models can account for the variation of S with the relative volume fraction of the metallic component in a binary system.[41,42] In conducting polymers, the thermoelectric power is more complicated than in binary systems, because metallic islands (corresponding to crystalline domains) are interconnected by disordered polymer chains in a complex manner, and because paracrystallinity exists in the metallic regions.[43] Contributions, distinguishable by their temperature dependence, to the thermoelectric power in conducting polymers are expected from (a) metallic crystalline domains and relatively well-organized chains in the disordered regions, $S_m(T) \propto T$;[17] (b) 3D VRH between metallic islands and between localized states, $S_{3D}(T) \propto \sqrt{T}$;[17] and (c) quasi-1D VRH in the disordered regions, $S_{1D}(T) \propto 1/T + \text{const.}$[29]

Commonly one of these contributing terms will be dominant for a given sample crystallinity and temperature range. For example, in highly crystalline samples, contributions to S from the metallic domains are expected to dominate at

high temperatures; on the other hand, in less crystalline ones the quasi-1D VRH term should dominate at low temperatures. Thus a generalized formula for $S(T)$ in conducting polymers of various crystallinity is a weighted summation of the above terms:

$$S(T)=\frac{\sigma_{1D}f_{1D}S_{1D}(T)+\sigma_{3D}f_{3D}S_{3D}(T)+\sigma_m f_m S_m(T)}{\sigma_{1D}f_{1D}+\sigma_{3D}f_{3D}+\sigma_m f_m}, \tag{3}$$

where f is the volume fraction and σ the conductivity assuming a constant thermal conductivity. The nonlinear thermoelectric power therefore can be fit by

$$S(T)=(A_1+A_2/T)+A_3\sqrt{T}+A_4T, \tag{4}$$

where A_1, A_2, A_3, and A_4 are effective coefficients related to the volume fractions and relative electrical conductivities of the material domains.

B. Microwave dielectric response of quasi-1D systems

The near-zero and room-temperature values of the microwave dielectric constant are important for estimates of the localization length and delocalization length scales in quasi-1D systems. The temperature dependence of the microwave conductivity and dielectric constant provides information about the charge delocalization mechanism in disordered systems. In this section, we introduce several theoretical models used for analysis of the microwave dielectric response.

1. Metallic box and interrupted metallic strands models

The metallic box model (MBM) (Refs. 29 and 44) and the interrupted metallic strands model (IMSM) (Ref. 45) represent the dielectric response of a quasi-1D metallic material at a finite frequency. Both models were developed in terms of linear metallic strands interrupted by insulating lattice defects. In the MBM these metallic strands are considered in bundles and treated as a metallic box. Near zero temperature the localization length (L) is the dimension of the metallic box, which we take as corresponding to the crystalline coherence length.[25] This model is useful to estimate L from the near-zero-temperature dielectric constant. For highly ordered materials (i.e., greater chain alignment in disordered regions) the model is applicable only at low temperatures. At higher temperatures phonon-induced delocalization present in the disordered regions can increase the size of the delocalized regions. Also, thermal energy can overcome the potential barriers in the disordered regions.

In the MBM the real part of dielectric constant (ϵ_r) is described as[29,44]

$$\epsilon_r=\epsilon_\infty+\left(\frac{2^{9/2}}{\pi^3}\right)e^2N(E_F)L^2, \tag{5}$$

where ϵ_∞ is due to core polarization, e is the electron charge, and $N(E_F)$ is the density of states at the Fermi level. Equation (5) can be used to estimate L at zero temperature. Assuming that $N(E_F)$ is temperature independent, one can estimate the scale of the charge delocalization as a function of temperature.

From the IMSM, the frequency and temperature dependence of the dielectric response can be predicted. The transient current in the IMSM, due to the response to an electric field $E(t)=E_0\theta(t)$, is[45]

$$I(t)=\theta(t)\sigma_0E_0\left[1-\exp\left(-\frac{t}{\tau_0}\right)\right]\exp\left(-\frac{t}{\tau_R}\right), \tag{6}$$

where σ_0 is the intrinsic metallic conductivity, τ_0 is the relaxation time without defects, and τ_R is the mean free time for the buildup of space-charge polarization effects at a constricting defect. The complex conductivity at a finite frequency is given by[45]

$$\sigma(\omega)=\frac{1}{E_0}\int_0^\infty dt\ \exp(i\omega t)\frac{\partial I(t)}{\partial t}$$
$$=i\omega\sigma_0\left[\frac{1}{(1-i\omega\tau)}-\frac{1}{(1-i\omega\tau_R)}\right], \tag{7}$$

where $\tau\equiv\tau_0\tau_R/(\tau_0+\tau_R)\equiv\lambda\tau_R$. In the low-frequency limit ($\omega\tau_R\ll1$), the real and imaginary parts of the complex dielectric constant are approximated as[45]

$$\epsilon_r\simeq1+\lambda\omega_p^2\tau_R^2 \tag{8}$$

and

$$\epsilon_i(\propto\sigma)\simeq\lambda(1+\lambda)\omega_p^2\omega\tau_R^3, \tag{9}$$

respectively. Here ω_p is the plasma frequency defined as $\omega_p^2=4\pi ne^2/m^*\epsilon_b$ where n is the carrier density, m^* is the effective mass, and ϵ_b is the background dielectric constant. Assuming that τ_R has a linear temperature dependence (such as $\tau_R\propto[\Omega T+\xi]$, where Ω is the increase of localization length per increase in temperature and ξ is a constant corresponding to the crystalline coherence length, i.e., zero-temperature localization length) the temperature dependence of ϵ_r and σ at low frequency will differ depending on the degree of disorder. For more ordered samples, the ΩT term in τ_R dominates, and $\epsilon(T)$ and $\sigma(T)$ at low temperatures (roughly $T\leqslant100$ K) are

$$\epsilon_r(T)\propto\tau_R^2\propto T^2 \tag{10}$$

and

$$\sigma(T)\propto\tau_R^3\propto aT^3+bT^2, \tag{11}$$

where a and b are the proportionality constants. For more disordered samples, the conduction electrons are not easily delocalized, and $\epsilon_r(T)$ and $\sigma(T)$ are weakly temperature dependent and described as

$$\epsilon_r(T)\propto T \tag{12}$$

and

$$\sigma(T)\propto cT^2+dT, \tag{13}$$

where c and d are the proportionality constants.

2. Model of Nakhmedov, Prigodin, and Samukhin

At high temperatures the conduction electrons become delocalized with increasing chain alignment in the disordered

regions. The interchain interaction is important for this delocalization. Nakhmedov, Prigodin, and Samukhin studied the dielectric response at a finite frequency, including the effects of interchain hopping.[46] This model considers more than one hop within the disordered regions. The complex conductivity in a quasi-1D conductor is described as[46]

$$\sigma(\omega, W_\perp) = \sigma_0 \left[\frac{W_\perp(T) - i\omega}{\nu} \right]^{1-2\gamma}, \tag{14}$$

where σ_0 is the intrinsic conductivity, ω is the frequency, $W_\perp(T)$ is the temperature-dependent interchain transfer rate, ν is the phonon frequency, and γ is the exponent defined below. The conductivity and dielectric constant in the limit of $\omega \ll W_\perp(T)$ are

$$\sigma \simeq \sigma_0 \left(\frac{W_\perp}{\nu} \right)^{1-2\gamma} \propto \epsilon_i \tag{15}$$

and

$$\epsilon_r \simeq \frac{1}{\omega} \left[\sigma_0 \left(\frac{W_\perp}{\nu} \right)^{1-2\gamma} (1-2\gamma) \left(\frac{\omega}{W_\perp} \right) \right] \simeq \frac{\sigma_0}{\nu} \left(\frac{\nu}{W_\perp} \right)^{2\gamma}, \tag{16}$$

where $\gamma \equiv (T/T_0) \ln[\nu/W_\perp(T)] \ll 1$ and T_0 is from the quasi-1D VRH model, i.e., $\sigma(T) \propto \exp[-(T_0/T)^{1/2}]$.[46] The interchain transfer rate $W_\perp$ can be written as

$$W_\perp = \nu (t_\perp \tau_\perp)^2 \exp\left[-\left(\frac{T_0}{T} \right)^{1/2} \right], \tag{17}$$

where $t_\perp$ is an interchain transfer integral and $\tau_\perp$ is the interchain hopping time. Therefore the temperature-dependent ϵ_r is deduced to be

$$\epsilon_r \propto \exp\left\{ \frac{T}{T_0} \left[\ln\left(\frac{1}{t_\perp \tau_\perp} \right) \right]^2 \right\}. \tag{18}$$

As the slope T_0 decreases (i.e., increasingly ordered chains in the disordered regions), the temperature dependence of ϵ_r exponentially increases. On the other hand, as T_0 becomes larger, the temperature-dependent ϵ_r is approximately that of a power law.

III. EXPERIMENTAL PRINCIPLES AND TECHNIQUES

The photographic method, which has the advantage of recording simultaneously the scattering intensity from several directions, was used to obtain the x-ray data. The cylindrical film, with the sample at its center, was placed in an evacuated chamber to reduce air scattering in order to perform long exposures. Cu $K\alpha$ ($\lambda = 1.542$ Å), monochromatic radiation, was used after (002) reflection of the incident x-ray beam on a doubly bent graphite monochromator. The photographic films were read using a microdensitometer in order to extract quantitative information on the x-ray percent crystallinity and coherence lengths of crystalline regions. The crystalline domain size or coherence length ξ is estimated from the ring's angular width $\Delta(2\theta)$ (full width at half maximum) using the Scherrer equation[43,47]

$$\xi = \frac{0.9\lambda}{\Delta(2\theta)\cos\theta}, \tag{19}$$

where λ is the x-ray wavelength and θ is the diffraction Bragg angle.

A four-probe technique was used to measure the dc conductivity in order to eliminate contact resistance. Four thin gold wires (0.05 mm in diameter) were attached in parallel to the sample surface with graphite paint (Acheson Electrodag 502) to ensure good electrical contact. The dissipative power was kept under 10^{-7} W to eliminate self-heating effects.

A two-probe method with a sandwich configuration was used to measure the variation of conductance at high electric fields, $\sigma(E)$. A HP214B pulse generator was used to generate high-voltage pulses with a maximum amplitude of 100 V. Considering the typical sample thickness was $\sim 20-30$ μm, the highest electric field applied to the sample was $\sim 5.0-3.3\times 10^4$ V/cm. Thin gold films were evaporated on the sample surfaces for electrical contact. Heating effects are detected by monitoring current variations within the duration of the voltage pulse. If time dependence occurred (caused by heating), the voltage pulse width or amplitude was reduced to eliminate these heating effects. The estimated temperature fluctuation at the sample was ± 0.2 K.

For measuring the thermoelectric power, a modified version of Chaikin's two-probe technique[48] was used. The free-standing films were attached between single crystal quartz blocks separated by ~ 3 mm. The sample chamber was kept under vacuum during the experiment to prevent heat conduction. The temperature difference across the sample during a measurement was typically $\leqslant 1$ K.

Microwave cavity perturbation[29,49] at 6.5 GHz and X-band (8.2–12.4 GHz) microwave impedance bridge techniques[50] were used for measuring the microwave dielectric constant (ϵ_{mw}) and conductivity (σ_{mw}). Advantages of the cavity perturbation method include its usefulness even when only small samples are available, and elimination of electrical and mechanical contact problems. When a small perturbation due to the insertion of a sample into the cavity is made, a small portion of microwave energy is absorbed by the sample, causing a change in the frequency and width of the cavity resonance. The resonance frequency shift and loss are $\delta = |f_{\mathrm{out}} - f_{\mathrm{in}}|/f_{\mathrm{out}}$ and $\Delta = (W_{\mathrm{in}} - W_{\mathrm{out}})/f_{\mathrm{out}}$, respectively, where f is the cavity resonance frequency, W is the cavity resonance width at half maximum, and the subscripts in and out correspond to the cavity with and without the sample, respectively.[51] The dielectric constant and conductivity are given by

$$\epsilon_{\mathrm{mw}} = 1 + \frac{[\delta(\alpha/N - \delta) - (\Delta/2)^2]}{N[(\Delta/2)^2 + (\alpha/N - \delta)^2]} \tag{20}$$

and

$$\sigma_{\mathrm{mw}} = \epsilon_0 \omega \frac{\alpha(\Delta/2)}{N^2[(\Delta/2)^2 + (\alpha/N - \delta)^2]}, \tag{21}$$

where N is the depolarization factor, ω is the angular resonance frequency, and α is the filling factor. The cavity method requires an accurate N when a rectangular sample is used. The results using the microwave impedance bridge

TABLE I. X-ray coherence length ξ of the various emeraldine hydrochloride (PAN-ES) and ''physically'' cross-linked emeraldine salt (XPAN-ES) films. Note that $\xi_{\perp}^{a}$, $\xi_{\perp}^{b}$, and $\xi_{\parallel}$ are obtained from $\Delta(2\theta)$ of (200), (010), and (002) ES-II reflections, respectively. H and L refer to high and low molecular weight samples, respectively. The stretching ratio (l/l_0) is given in parentheses (e.g., 3.5×). Also shown is the percent of crystallinity determined in the equatorial direction ($X_c^{\perp}$).

Materials	ξ (Å)			
	$\xi_{\parallel}$	$\xi_{\perp}^{b}$	$\xi_{\perp}^{a}$	$X_c^{\perp}$
A: Intermediate XPAN-ES^H (3.5×)	73	57	31	0.46±0.10
B: High XPAN-ES^H (3.5×)	64	47	25	0.40±0.10
C: High XPAN-ES^L (5.5×)	57	45	24	0.37±0.10
D: PAN-ES^L (4×)	52	43	28	0.30±0.10
E: ''amorphous'' PAN-ES^L (1×)		~15		≤0.10

method are well suited for an independent determination of the depolarization factor of a rectangular sample for use in the analysis of the cavity perturbation results.[50] A detailed description of the bridge method used to determine σ_{mw} and ϵ_{mw} is given in Ref. 50.

The EPR spectra were obtained using a Bruker Instruments ESP300 (X-band) electron paramagnetic resonance spectrometer fitted with a TE102 resonant cavity. Temperature control from 5 to 300 K was achieved using an Oxford 900 continuous flow helium cryostat. Samples were loaded unoriented[52] into sealed quartz EPR tubes with helium gas for thermal exchange.

IV. MATERIALS AND EXPERIMENTAL RESULTS

A. Physically cross-linked polyaniline materials

For the present work four partially crystalline films (samples A, B, C and D; see Table I) and one ''amorphous'' film (sample E) of fully HCl doped ($Cl^-/N \simeq 49 \pm 2\%$) emeraldine salt form of polyaniline (PAN) were studied. Samples (A, B, and C) were prepared using a gel process, described below, which resulted in varying degrees of ''physical'' cross-linking; these samples are denoted as XPAN-ES. Samples D (data previously reported by Wang *et al.*[29]) and E were prepared using processes where gelation did not occur; these samples are denoted as PAN-ES.

XPAN-ES films, samples A and B, were prepared using high molecular weight (MW) (~120 000 g mol^{-1}) EB.[38] This high-MW EB was dissolved in N-methylpyrrolidinone (NMP) and filtered to make a 3-wt % solution and subsequently cast onto glass substrates. The differences in the degree of ''physical'' cross-linking observed between samples A and B were due entirely to conditions under which the films were dried. For sample A, the EB-NMP solution was cast onto a glass substrate and subsequently placed inside a convection oven at ~50 °C and allowed to dry for ~15 h. For sample B, the same EB-NMP solution was cast onto a glass substrate and placed inside a plastic reservoir sealed to control evaporation of NMP and allow gelation. After one week the film was removed from the plastic reservoir, placed in an oven at ~60 °C, and dried under a constant flow of nitrogen gas. This resulted in a highly cross-linked PAN-EB film. Sample C was prepared in a manner similar to sample B using a 3-wt % solution in NMP although using a lower MW (≤70 000 g mol^{-1}) EB. These samples (A–C) were stretched using a zone drawing method[53] where the film was stretched between two heated copper wires (T>140 °C). The stretch ratio was controlled by the temperature and force applied by the copper wires. The emeraldine salt form of polyaniline was obtained by immersing stretched EB films in HCl ($pH \simeq 0$) for ~48 h. The term ''physically crosslinked'' refers to increased structural local order among the chains, not covalent chemical bonding. The degree of ''cross-linking'' is controlled by the appropriate choice of the MW, gelation time, and concentration of the EB-NMP solution.

The ''partially'' crystalline PAN-ES films, sample D, was prepared from low molecular weight (MW≤70 000 g mol^{-1}) emeraldine base. Films were cast from solutions of EB dissolved in NMP on glass, dried in a vacuum oven at ~50 °C for ~24 h, and removed from the glass by immersion in distilled water. Subsequently, the films were stretched up to four times using a uniaxial web stretching device. The technique uses two rollers in series where stretching takes place at the first roller held at 148 °C and the second roller held at 100 °C is used to anneal the film.

The ''amorphous'' PAN-ES films, sample E, was prepared from low molecular weight (MW≤70,000 g mol^{-1}) emeraldine base (EB). This low-MW EB was dissolved in NMP and filtered to make a homogeneous 1–3-wt % solution. The solution was then cast on a glass substrate and the solvent removed quickly, to prevent gelation, by a rapid stream of room temperature air. Approximately 15 wt % of NMP was permitted to remain in the films to act as a plasticizer. The resulting PAN-EB films were completely soluble in NMP and essentially amorphous with no cross-linking present. In addition to the unstretched PAN-ES film (sample E), a 12.5 times stretched version was prepared by zone drawing at 180 °C. The doped PAN-ES form of these films was obtained by immersion in aqueous HCl ($pH \simeq 0$) for ~48 h.

B. X-ray structure

Figures 1(a)–1(e) show x-ray patterns from stretched XPAN-ES (samples A, B, and C), stretched PAN-ES (sample D), and unstretched PAN-ES (sample E). A microdensitometer reading of these x-ray patterns in the equatorial (i.e., within the plane perpendicular to the stretching direction) is shown in Fig. 1(f). Samples A–D are partially crystalline with the degree of crystallinity decreasing from sample A–D. Listed in Table I are the percent of crystallinity in equatorial directions ($X_c^{\perp}$) estimated from the ratio of the integrated intensity of the sharp reflections above the amorphous halo to the total scattered intensity using the microdensitometer readings of Fig. 1(f). $X_c^{\perp}$ decreases from sample A to sample E, where E is essentially amorphous.

The crystalline regions of samples A–D have the ES-II structure, while the quasi-amorphous sample, E, exhibits the ES-I local order.[54] The x-ray patterns of samples A–D (shown in Fig. 1) can be completely indexed using the ES-II structure. The x-ray pattern of sample A is indexed in Fig. 6(b) of Ref. 55. The ES-II indexation also is given on the microdensitometer reading for the equatorial directions of sample A, Fig. 1(f).

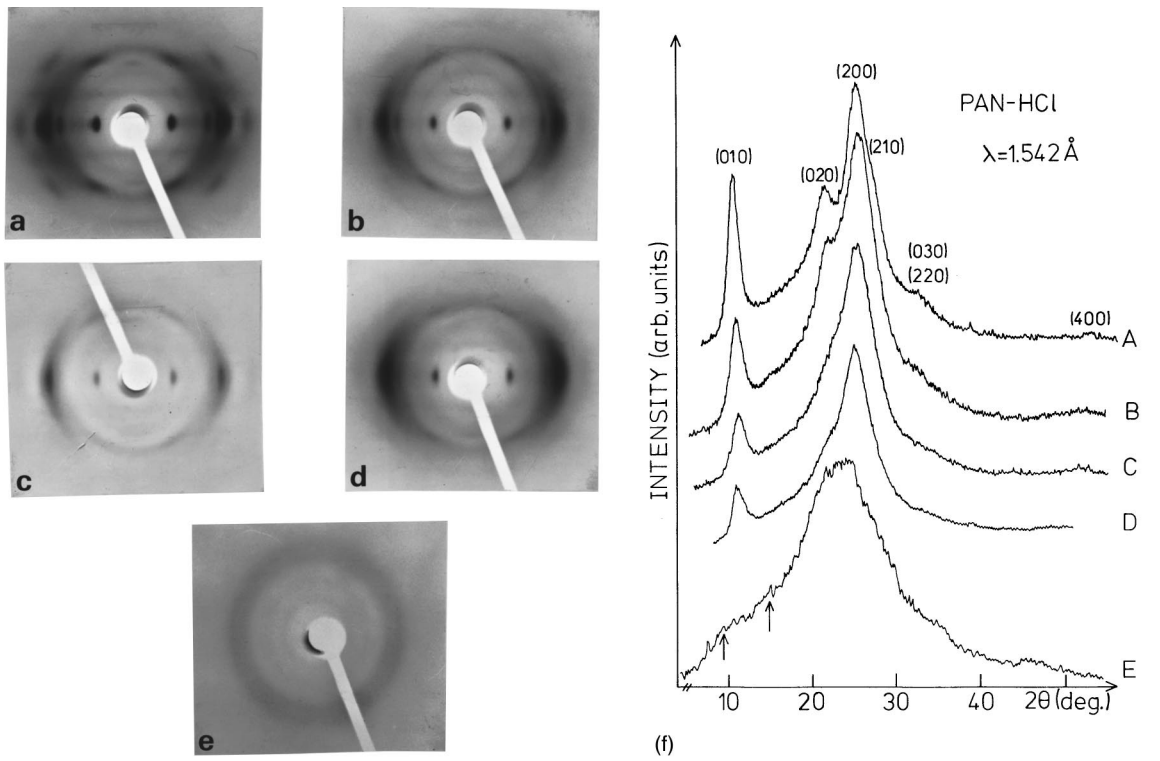

FIG. 1. (a)–(e) X-ray patterns from samples A, B, C, D, and E, respectively ($\lambda = 1.542$ Å). The stretching direction of samples A–D is vertical. (f) The x ray from diffraction intensity vs 2θ microdensitometer readings of samples A–E in the equatorial direction. The microdensitometer reading of sample A has been indexed with the ES-II orthorhombic frame. The arrows point toward the position of the two broad peaks characteristic of ES-I local order, for the microdensitometer reading of sample E.

The ES-II chain array can be accounted for by the P_{c2a} or B_{m2m} orthorhombic space groups, where for sample A the lattice parameters are $a = 7.0$ Å and $b = 8.2$ Å in the equatorial directions, and $c = 10.4$ Å in polymer chain direction. The lattice parameter b is slightly sample dependent, being 8.05 Å for samples B and D and 7.9 Å for sample C. The ES-I structure is less accurately known and has a lower (monoclinic or triclinic) symmetry. In the case of sample E the ES-I local order can be easily identified by the presence of two broad reflections at small Bragg angles, i.e., $2\theta \sim 9.5°$ and $\sim 15°$ or $d \sim 9.3$ and ~ 5.9 Å, respectively [arrows, Fig. 1(f)].

Figure 1(f) shows that the (010), (020), and (200) ES-II reflections progressively broaden and decrease in intensity from samples A to D. Also, it is evident that the change is less important for the strongest (200) reflections. The x-ray patterns of samples C and D are very similar. The crystalline domain size or coherence length (ξ) can be estimated from the angular width $\Delta(2\theta)$ of some of the well-defined reflections using the Scherrer equation (19).

The coherence lengths $\xi_{\perp}^{a}$, $\xi_{\perp}^{b}$, and $\xi_{\parallel}$ of samples A–D have been deduced from the width of the (200), (010), and (002) ES-II reflections, respectively. For sample E, an isotropic ξ was estimated from the width of the two broad halos at small θ shown by arrows in Fig. 1(f). These values are listed in Table I (error estimated at ± 5 Å) and show ξ basically decreasing from sample A to E.

The wide range of local order or crystallinity in polyaniline depends upon the details of the chemical processing, such as the degree of crosslinking, molecular weight and stretch ratio. With this in mind high molecular weight XPAN-ES samples can be divided into two categories: (a) those doped in the unstretched form are poorly crystallized, which exhibit the ES-I local order;[56] and (b) those doped in the stretched form, which show improved crystallinity and the ES-II chain array. Samples A and B belong to the second category. However, it is evident (Table I) that the crystallinity of the highly cross-linked sample B is less improved by stretching than is the intermediate cross-linked sample A. This probably results from the greater rigidity of the polymer chains in the highly crosslinked material. In contrast, the low molecular weight XPAN-ES sample, doped in the unstretched form exhibits a medium crystallinity and the ES-II chain array structure.[57] However, its crystalline features were not substantially improved by doping in the stretched form (sample C). Table I shows that in spite of a higher degree of stretching the highly cross-linked sample C is slightly less crystalline than the highly cross-linked sample, B, which has a higher molecular weight. Also from Table I the low molecular weight standard PAN-ES (sample D) is slightly less crystalline than the low molecular weight high XPAN-ES (sample C). However, these two families have quite different crystallinity in their doped unstretched form: while unstretched XPAN-ES exhibits a medium crystallinity and the ES-II chain array structure, the unstretched PAN-ES is strongly disordered with the ES-I local order. The low molecular weight PAN-ES unstretched material sample E also is strongly disordered (nearly completely amorphous) with only very limited ES-I local order. However, it differs from the other samples in that this strongly disordered state is

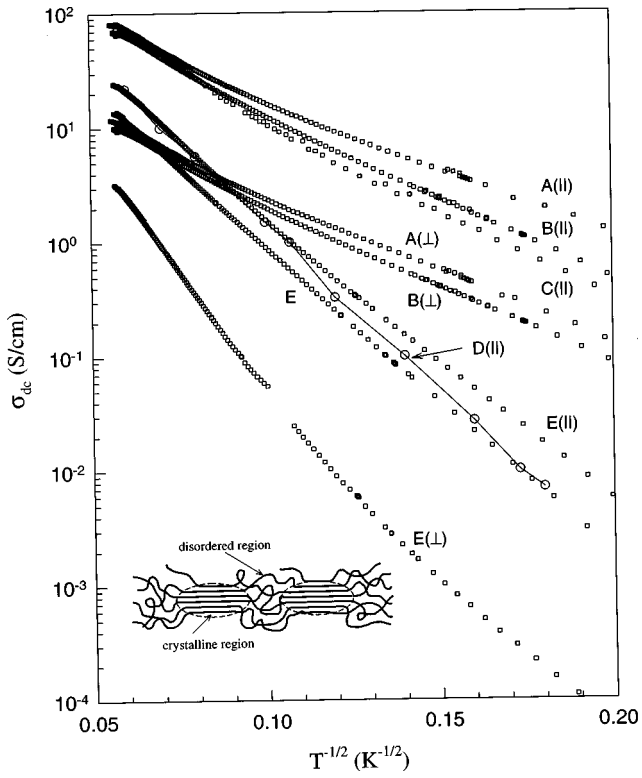

FIG. 2. $\ln \sigma_{dc}$ vs $T^{-1/2}$ of dc conductivity of HCl doped XPAN-ES and PAN-ES samples in both parallel and perpendicular directions. Data for sample D($\|$) are from Ref. 29. Inset: Schematic representation of inhomogeneous disorder model for polyaniline; 3D crystalline regions are coupled into a 3D network by single chains passing through the disordered regions (from Ref. 25).

maintained in the doped 12.5× stretched form in spite of a change from ES-I to ES-II local order.

C. Direct current and high-electric-field-dependent conductivity

The temperature dependence of the dc conductivity, $\sigma_{dc}(T)$, for the XPAN-ES and PAN-ES samples is shown in Fig. 2 plotted as $\log_{10} \sigma$ vs $T^{-1/2}$ for comparison with the quasi-1D VRH model. The inset in Fig. 2 is a schematic representation of the inhomogeneous disorder model for polyaniline, where 3D crystalline regions are coupled to form a 3D network by single chains passing through the disordered regions. The values of T_0 based on fits to the quasi-1D VRH model are listed in Table II. Note that for samples A($\|$), B($\|$), and C($\|$), the model holds for temperatures below ~100 K, while for samples D($\|$) and unstretched E it provides the best fit over the entire temperature range. *As the crystallinity or coherence length increases,* T_0,

TABLE II. Slope T_0 [fit to Eq. (1)] of the temperature-dependent dc conductivity of the various XPAN-ES and PAN-ES samples in parallel and perpendicular directions. Note that sample E, used for the T_0 measurement, was stretched 12.5 times.

Materials	A	B	C	D	E
$T_0(\|)$ (K)	700	900	1000	4300	3800
$T_0(\perp)$ (K)	870	990	not measured	5200	9800

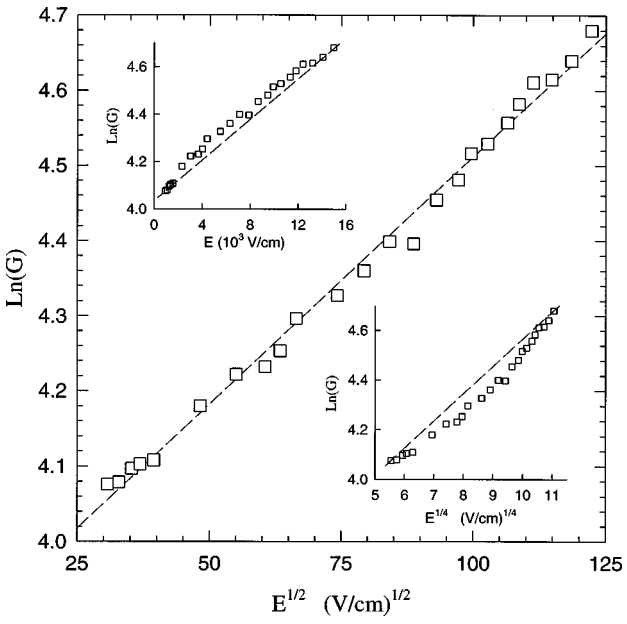

FIG. 3. Electric-field-dependent conductance of sample B at 62 K measured using a two-probe method. The data are plotted as $\ln(G)$ vs $E^{1/2}$, where $G=A\sigma/l$ and A and l are dependent on the sample geometry. Insets are plots of $\ln(G)$ vs E and $\ln(G)$ vs $E^{1/4}$ for comparison to Eq. (2).

the effective energy separation between localized states, decreases. This implies that polymer chains in disordered regions also are more coherently aligned in accordance with the results of the x-ray scattering experiments. This suggests that in the samples with the highest crystallinity the localized charges in the disordered regions can more readily delocalize over several metallic islands. This may cause the deviation of $\sigma_{dc}(T)$ from the quasi-1D VRH model observed in samples A($\|$), B($\|$), and C($\|$) above ~100 K. Also the anisotropy in the conductivity of the stretched samples was $\sigma_{dc}(\|)/\sigma_{dc}(\perp) \geqslant 5$ over the measured temperature range.

The T-dependent parallel and perpendicular $\sigma(T)$ of HCl doped 12.5 times stretched sample E was also studied (Fig. 2). While $\log(\sigma_{\|})$ is still proportional to $T^{-1/2}$ over the entire temperature range with $T_{0,\|} \sim 3800$ K, essentially unchanged from the isotropic value ($T_{0,\text{isotropic}} \sim 3800$ K), the conductivity $\sigma_{\|}$(300 K) has increased approximately twofold compared to the room-temperature conductivity of the unstretched sample. Similarly, $\log(\sigma_{\perp})$ above ~100 K is also proportional to $T^{-1/2}$; however, $T_{0,\perp}$ is approximately 9800 K, consistent with $\sigma_{\perp}$(300 K), almost four times smaller than the conductivity at room temperature of the unstretched sample, and roughly one order of magnitude smaller than $\sigma_{\|}$(300 K).

The electric-field-dependent conductance $G(E)$ of sample B at a constant temperature of 62 K in the region of quasi-1D VRH was measured. The data are plotted in Fig. 3 as $\ln(G)$ vs $E^{1/2}$ [$\ln(G)$ vs E and $E^{1/4}$ are inset in Fig. 3 for comparison to Eq. (2)] where the conductance is related to the conductivity by geometric factors, i.e., $G=A\sigma/l$, where A is area and l is length. The data in Fig. 3 is nearly linear for $1/(1+d)=\frac{1}{2}$, consistent with the quasi-1D VRH model. However, compared to the linear regression line (dashed line in Fig. 3) the data show a slight negative concavity. The best

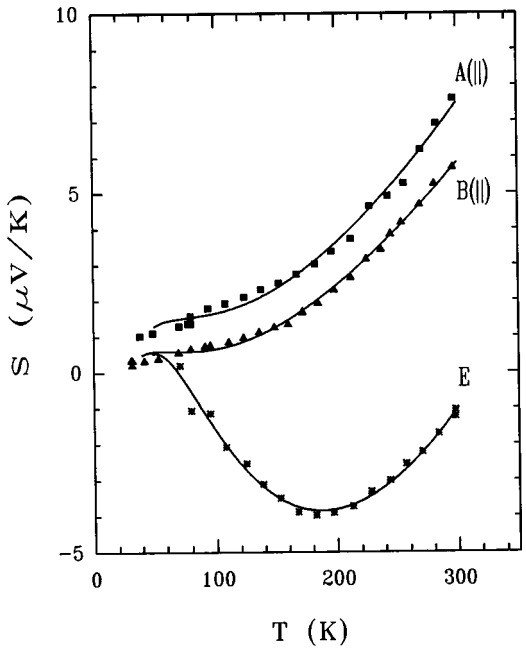

FIG. 4. Thermoelectric power of selected XPAN-ES samples as a function of temperature. The solid lines are guides to the eye for comparison with Eq. (4).

fit of the data to Eq. (2) gives $1/(1+d)=0.67$ still in good agreement with the quasi-1D VRH model.

D. Thermoelectric power

The temperature dependence of the thermoelectric power, $S(T)$, for the two most highly crystalline samples, A($\|$) and B($\|$), and the least crystalline sample, E, are shown in Fig. 4. The positive thermoelectric power observed in samples A($\|$) and B($\|$) imply a net p-type conduction mechanism. Also for these two samples, $dS(T)/dT$ continuously increases above $\sim$150 K, which may reflect phonon induced charge delocalization. For the most disordered sample E, $S(T)$ is negative except at temperatures $\leqslant$80 K. Also, $S(T)$ shows a complex temperature dependence with a positive slope, $dS(T)/dT$, for $T\geqslant$200 K, and a minimum at $\sim$200 K. For sample E, the percent crystallinity and crystalline domain size are negligibly small compared with the more crystalline samples. Thus contributions to the thermoelectric power from the disordered regions will dominate, possibly accounting for the reduced S above $\sim$200 K and the change in sign. The important result is that the temperature-dependent thermoelectric power becomes increasingly metal-like ($S_m \propto T$) as the crystallinity increases.

Shown in Fig. 4 as the solid curves are the fits of Eqs. (4) to the experimental $S(T)$ for samples A($\|$), B($\|$), and E. Good fits over the entire measured temperature range are obtained for all three of these samples. The coefficients A_1, A_2, A_3 and A_4 are listed in Table III. Comparing these coefficients, the sign of each term in Eqs. (4) is the same across all three samples. The contribution to the thermoelectric power in sample E from quasi-1D and 3D VRH are relatively large compared to that of the two more crystalline samples, indicating that in less crystalline materials the thermoelectric power is dominated by contribution from the disordered regions.

TABLE III. Effective temperature coefficients A_1, A_2, A_3, and A_4 of thermoelectric power of XPAN-ES samples.

Materials	A_1 (μV K^{-1})	A_2(μV)	A_3 (μV K$^{-3/2}$)	A_4 (μV K^{-2})
A($\|$)	20.2	−247	−2.87	0.126
B($\|$)	14.2	−147	−2.23	0.103
E	56.8	−738	−7.72	0.261

It is noted that the ratio of A_2 to A_1 is nearly the same for samples A($\|$), B($\|$), and E (see Table III) implying that the ratio of intrachain to interchain contributions to the thermoelectric power is approximately constant for regions of these samples, where quasi-1D VRH dominates. The largest linear (''metallic'') contribution for the least conducting sample (E) may reflect the proportionality of the metallic contribution to

$$\frac{d\ \ln\sigma(E)}{dE}=\frac{1}{\sigma}\frac{d(ne\mu)}{dE}=\frac{1}{\sigma}\left[ne\left(\frac{\partial\mu}{\partial E}\right)+\mu e\left(\frac{\partial n}{\partial E}\right)\right]. \tag{22}$$

Here n is the charge carrier density, μ their mobility, and E the energy. The narrower bandwidth for the more disordered samples would then lead to larger $\partial\mu/\partial E$ and $\partial n/\partial E$ terms and therefore a larger ''metallic'' thermoelectric power.

E. Microwave conductivity and dielectric constant

Figure 5 shows the temperature dependence of the 6.5-GHz dielectric constant, $\epsilon_{\rm mw}(T)$, for the XPAN-ES and PAN-ES samples below 100 K. The value of $\epsilon_{\rm mw}$ at 100 K increases with increasing sample crystallinity. In samples A($\|$), B($\|$), and C($\|$), $\epsilon_{\rm mw}(T)$ is approximately $\propto T^2$ and for samples D($\|$) and E it is roughly $\propto T$ (for $T\leqslant$100 K). In this regime we apply the IMSM in the low-frequency limit [Eqs. (8) and (9)], assuming the charge motion is confined to isolated metallic islands and the energy is insufficient to overcome the disordered potential barriers between metallic

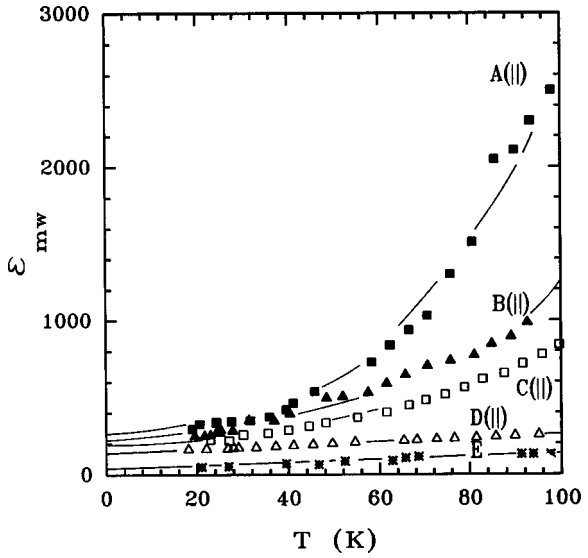

FIG. 5. Temperature dependence of the microwave dielectric constant $\epsilon_{\rm mw}$ of XPAN-ES and PAN-ES samples at low temperature ($T\leqslant$100 K). The solid curves are guides to the eye.

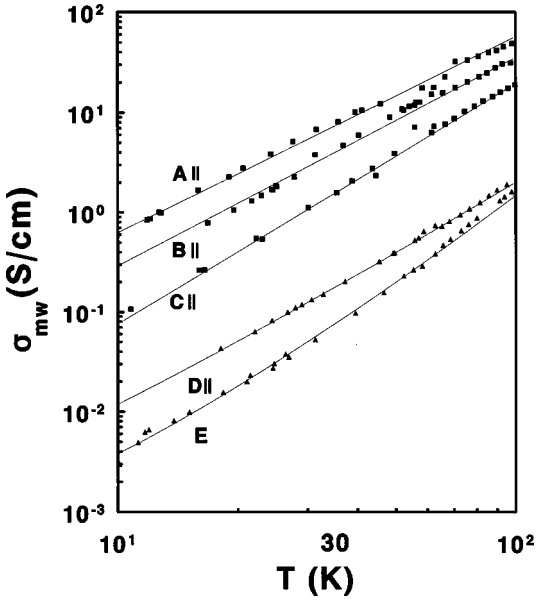

FIG. 6. Temperature-dependent microwave conductivity $\sigma_{\mathrm{mw}}(T)$ of XPAN-ES and PAN-ES materials at low temperature ($T \leqslant 100$ K). The solid lines are curves for comparison with the interrupted metallic strand model (IMSM).

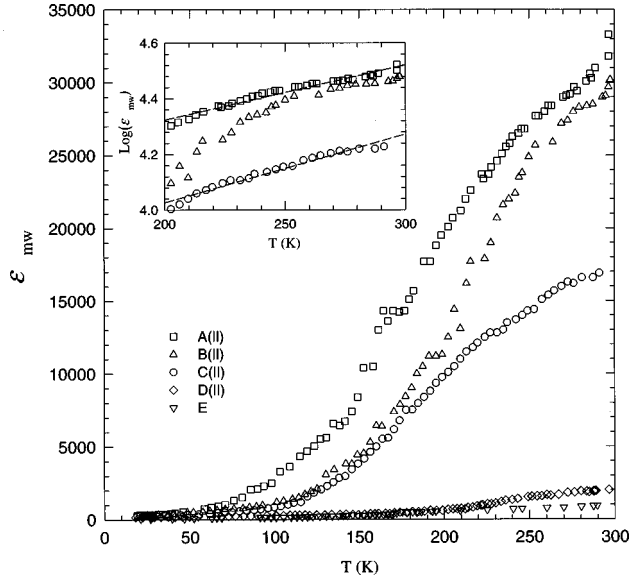

FIG. 7. The comparison of microwave dielectric constant $\epsilon_{\mathrm{mw}}(T)$ in the parallel direction for XPAN-ES and PAN-ES samples. Inset: $\ln(\epsilon_{\mathrm{mw}})$ vs T for $T \geqslant 200$ K; the linear regression lines (dashed lines) for samples A and C are shown for comparison to $\tau_\perp$ of the model of Ref. 46.

islands. Assuming $\tau_R \propto (\xi + \Omega T)$, the IMSM predicts $\epsilon_{\mathrm{mw}} \propto T^2$ for highly crystalline materials [samples A($\|$), B($\|$), and C($\|$)], and $\epsilon_{\mathrm{mw}} \propto T$ for less crystalline materials [samples D($\|$) and E]. This is in agreement with the low-temperature $\epsilon_{\mathrm{mw}}(T)$ data, and directly demonstrates the central role of processing-induced local order in developing the metallic state. Based upon the MBM,[44] the increase in ϵ_{mw} as $T \to 0$ implies that the size of the metallic islands (or localization length, L) increases in accord with the x-ray diffraction results. The expansion of the metallic regions with increasing temperature is consistent with the presence of more coherently organized chains between metallic islands.

A logarithmic plot of the temperature dependent microwave conductivity, $\sigma_{\mathrm{mw}}(T)$, of samples A–E for $T \leqslant 100$ K, is shown in Fig. 6. The slopes are $\simeq 2.0$, $\simeq 2.1$, and $\simeq 2.4$ S K cm^{-1} for more ordered samples A($\|$), B($\|$), and C($\|$), respectively, and ~ 2.1 S K$\cdot$cm^{-1} for the least ordered samples (sample E) showing that the T^2 term dominates, consistent with the IMSM. However, for sample E above 25 K and sample D above 15 K, the slopes are ~ 2.3 and ~ 3.0, respectively. These values are larger than expected for the IMSM, and suggest that for poorly conducting samples a few well ordered chains with large Ω may make a large contribution to the observed temperature dependence of the microwave conductivity.

The temperature dependence ($\leqslant 300$ K) of the microwave dielectric constant for the XPAN-ES and PAN-ES samples are shown in Figs. 7 and 8 for orientations parallel and perpendicular to the chain direction. The anisotropy in the microwave dielectric constant, $\epsilon_{\mathrm{mw}}(\|)/\epsilon_{\mathrm{mw}}(\perp)$, at room temperature is ~ 10 for samples A, B, and C. The room-temperature value of $\epsilon_{\mathrm{mw}}(\|)$ dramatically increases from ~ 800 for the most disordered sample (E) to $\sim 3.3 \times 10^4$ for the highest crystalline XPAN-ES. The room-temperature values of $\epsilon_{\mathrm{mw}}(\|)$ for samples A, B, and E were confirmed using a microwave impedance bridge method. For example, in sample B at room temperature $\epsilon_{\mathrm{mw}}(\|)$ was $\simeq 2 \times 10^4$ to 3×10^4 from the X-band (8.2–12.4 GHz) impedance bridge experiments. As the crystallinity increases, $\epsilon_{\mathrm{mw}}(T)$ changes from a power law to a nearly exponential temperature dependence.

The model of Ref. 46, which considers more than one hop at a finite frequency, has been used to interpret ϵ_{mw} at high temperatures (T roughly $\geqslant 100$ K). This theory predicts $\epsilon_{\mathrm{mw}} \propto \exp(T/T_0[\ln(1/t_\perp \tau_\perp)]^2)$, where T_0 is the slope of the temperature-dependent dc conductivity, $t_\perp$ is the interchain charge transfer integral, and $\tau_\perp$ is the interchain hopping time. Because of the small T_0 in samples A($\|$), B($\|$), and C($\|$), ϵ_{mw} has an exponential temperature dependence. From the inset in Fig. 7, which is the extended scale of $\epsilon_{\mathrm{mw}}(T)$ for $T \geqslant 200$ K, the interchain hopping time $\tau_\perp$ is determined to be $\sim 10^{-15}$ s for both samples A($\|$) and C($\|$), assuming $t_\perp = 0.3$ eV. It is noted that this value of τ (10^{-15} s) is the same order as τ determined in fitting the optical conductivity for the more localized charge carriers of camphorsulfonic-acid-doped polyaniline.[22] However, in the lower crystalline samples with large T_0, $\epsilon_{\mathrm{mw}}(T)$ can be approximated by a power law. The previous and present measurements of $\epsilon_{\mathrm{mw}}(T)$ for sample D($\|$) show a $\epsilon_{\mathrm{mw}}(T) \propto T^2$ behavior.[29] The exponential increase in $\epsilon_{\mathrm{mw}}(T)$ and its large positive value ($> 10^4$) at room temperature support the increase in size of the metallic regions and more coherent chain alignment in the disordered regions. In less crystalline materials, the charge delocalization is not effective because the irregular and high potential barriers interrupt the charge delocalization.

F. Electron paramagnetic resonance

In this section we report measurements of the EPR temperature dependence for samples A and E, the highest (3.5 times stretched) and lowest (unstretched) crystalline samples,

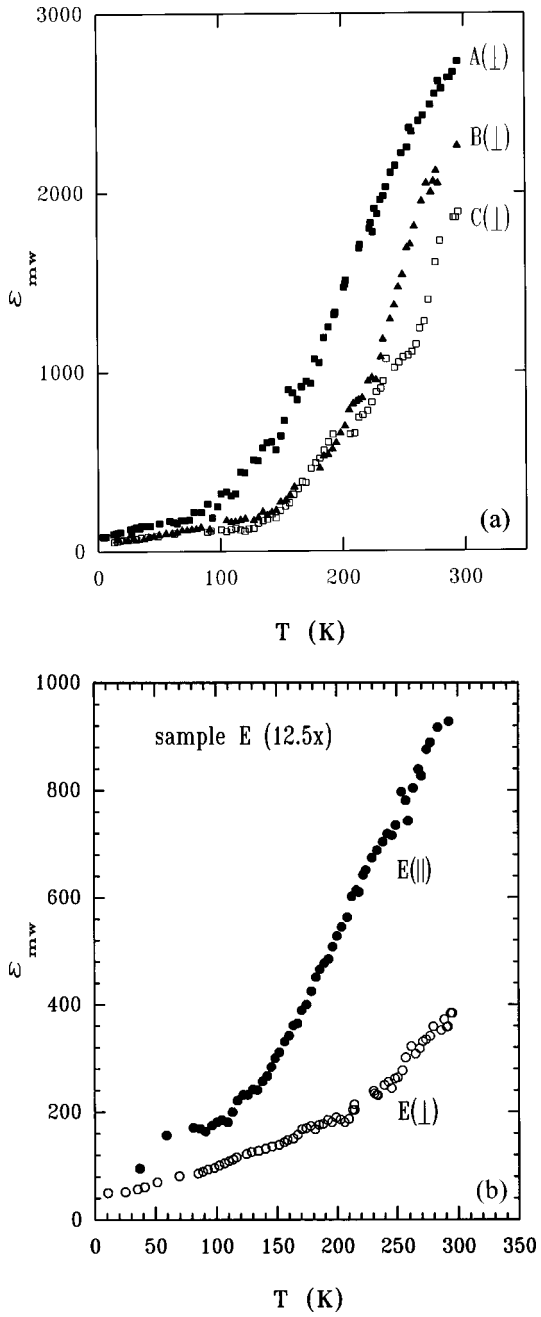

FIG. 8. (a) The comparison of microwave dielectric constant $\epsilon_{\mathrm{mw}}(T)$ in the perpendicular direction for XPAN-ES samples. (b) $\epsilon_{\mathrm{mw}}(T)$ in the parallel and perpendicular directions for doped 12.5 times stretched sample E.

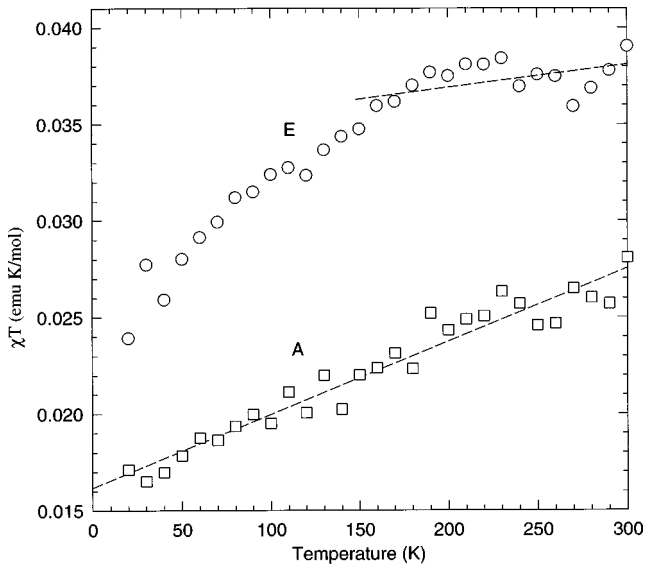

FIG. 9. Plots of χT vs temperature for samples A and E, where χ is estimated based on the EPR-integrated intensities referenced to a $Cu^{II}SO_4\ 5H_2O$ standard. The dashed lines estimate the average slope over the temperatures range where the linewidth increases linearly with T, ~20–300 and ~150–300 K, for samples A and E, respectively.

respectively. The g values of both samples are ~2.0032 from room temperature to 30 K. The susceptibility of samples A and E have been estimated from the EPR-integrated intensities calibrated against a $Cu^{II}SO_4\ 5H_2O$ standard, and are plotted in Fig. 9 as χT vs T. Assuming the total susceptibility (χ) is composed of a Pauli (χ_P) and Curie ($\chi_C = C/T$ where C is the Curie constant) component, linear fits to χT (Fig. 9, dashed lines) over the temperature range for which the linewidth increases linearly with T (20–300 K for sample A, 150–300 K for sample E) give $\chi_P[\mathrm{A}] = 3.77\times10^{-5}$ emu mol^{-1}, $\chi_P[\mathrm{E}] = 1.2\times10^{-5}$ emu mol^{-1}, $C[\mathrm{A}] = 0.0162$ emu K mol^{-1}, and $C[\mathrm{E}] = 0.035$ emu K mol^{-1}. A molecular weight of 250.72 g mol^{-1} is used corresponding to a two ring unit of PAN-ES, and includes a 15-wt % NMP content. From χ_P the average density of states at the Fermi energy for the two samples is estimated to be $N(\epsilon_F)[\mathrm{A}] = 1.17$ states (eV per two-rings)$^{-1}$ and $N(\epsilon_F)[\mathrm{E}] = 0.37$ states (eV two-rings)$^{-1}$. Similarly, the density of Curie spins is estimated to be 0.043 and 0.092 spins per two-rings for samples A and E, respectively.

In general EPR line shapes (i.e., linewidths) are determined by spin-spin (hyperfine, dipolar, etc.) interactions, narrowing mechanisms (spin diffusion, rotation, and exchange) and spin-lattice relaxation. In systems that do not have complicated line shapes, i.e., homogeneously broadened (Lorentzian) lines, the spin-spin interactions and effects of any narrowing mechanisms can be described in terms of an effective spin-spin relaxation time T_2. For an EPR spectrum with a Lorentzian line shape, the half-width at half maximum linewidth can be written

$$\Delta H = \gamma^{-1}\left(\frac{1}{T_2} + \frac{1}{2T_1}\right), \tag{23}$$

where γ is the gyromagnetic ratio and T_1 is the spin-lattice relaxation time.[58] In conducting polymers the hyperfine and dipolar broadening of a resonance will be limited by narrowing due to spin diffusion.[59] Thus increases in conductivity will increase the effectiveness of spin diffusion to narrow the EPR linewidth. This is reflected as a decrease in T_2^{-1}.

The conductivity at room temperature of sample A(∥) is roughly an order of magnitude larger than in sample E and at low temperatures roughly two orders of magnitude larger. Assuming the hyperfine and dipolar interactions in these samples are the same, it follows that the $1/T_2$ contribution to the total linewidth will be smaller in sample A than in sample E. However, the experimental linewidths of sample A are 3–8 times larger than those of sample E for the entire

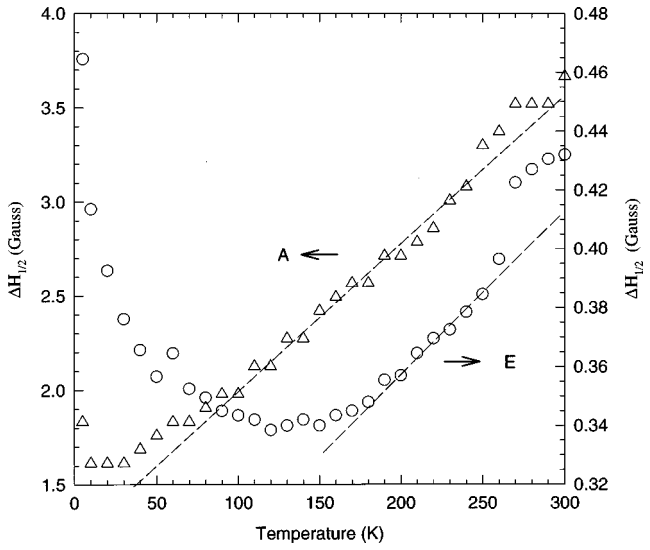

FIG. 10. Plots of the half-width at half maximum linewidth vs temperature for samples A and E. The dashed lines are drawn to emphasize the linear temperature dependence.

temperature range (Fig. 10). Further, from $\sigma(T)$ the $1/T_2$ linewidth contribution for both samples should decrease with increasing temperature. However, only in sample E below 150 K is the linewidth's temperature dependence consistent with a $1/T_2$-dominated linewidth. In sample A above 40 K, and in sample E above 150 K, we observe a linewidth which increases roughly linearly with temperature consistent with a $(1/2T_1)$-dominated linewidth. In Fig. 10, the estimated slopes (dashed lines) of $\Delta H(T)$ are 7.7×10^{-3} and 6.7×10^{-4} G K^{-1} for samples A and E, respectively. The line shapes for both samples are Lorentzian consistent with 3D spin diffusion as opposed to lower-dimensional line shapes reported for lower conductivity polyaniline and polyaniline derivatives.[29,60,61]

A possible explanation is that the faster relaxation time, T_1, in sample A relative to sample E, and its Lorentzian line shape, may be explained in terms of spin-spin interaction between the *conduction electrons* of the metallic islands and the localized spins of *localized polarons* in the surrounding disordered regions giving rise to added relaxation routes. Earlier coordinated magnetic and x-ray-diffraction studies showed the localized states in the disordered regions of partially crystalline HCl-doped polyaniline were primarily spinless bipolarons.[43] Therefore, in the higher crystalline materials, such as sample A, a few localized polarons in the disordered regions may dominate the magnetic relaxation. Thus a modest density of localized polarons (0.043 and 0.092 spins per two rings for samples A and E, respectively) would dominate the relaxation process in these materials. The dynamical properties for systems containing magnetic ions in metals where localized spins and conduction electrons interact via exchange have been studied in terms of the modified Bloch equations of motion proposed by Hasegawa.[62] Assuming the isothermal limit,[63] the effective spin-lattice relaxation is roughly given by the Korringa relaxation rate. Thus $\Delta H\propto N^2(E_F)T$, where $N(E_F)$ is the density of states at the Fermi energy, and the linewidth is expected to increase linearly with temperature in this region

TABLE IV. Room-temperature effective delocalization length $L_{\rm eff}$(RT) of XPAN-ES and PAN-ES samples determined from $\epsilon_{\rm mw}$(RT).

Materials	$L_{\parallel,\rm eff}$(RT) (Å)	$L_{\perp,\rm eff}$(RT) (Å)
A	1200	350
B	1200	330
C	880	300
D	300	120
E	210	

consistent with Fig. 10. Further, using the $N(E_F)$[A] and $N(E_F)$[E] values obtained from Fig. 9 and $d(\Delta H)/dT \propto N^2(E_F)$, it follows that

$$\frac{d\Delta H[A]}{dT}\left(\frac{d\Delta H[E]}{dT}\right)^{-1}=\left(\frac{N(E_F)[A]}{N(E_F)[E]}\right)^2\sim 10. \qquad (24)$$

This is roughly consistent with the ratio of the slopes of $\Delta H(T)$, obtained from Fig. 10, of

$$\frac{d\Delta H[A]}{dT}\left(\frac{d\Delta H[E]}{dT}\right)^{-1}=11.5. \qquad (25)$$

Summarizing the EPR study, the density of states and density of Curie spins determined for samples A and E are in agreement with the earlier studies showing metallic Pauli susceptibility in the ordered regions and predominantly spinless bipolarons with occasional polarons in the disordered doped polyanilines. At low temperatures (<40 K for sample A and <140 K for sample E), T_2 processes appear to dominate due to EPR linewidth narrowing with increasing temperature. For higher temperatures a Korringa relaxation mechanism between conduction electrons and localized polarons could account for the linear increase in linewidth with increasing temperature and the anomalously larger linewidth for the more conductive sample. Further, the known three-dimensional delocalization of the conduction electrons[19,25] is in agreement with the Lorentzian line shape observed.

V. DISCUSSION

In this section, we discuss the mesoscopic metallic states of the highest crystalline HCl-doped polyanilines based upon the nature of the metallic states of the ordered (or metallic) regions and the charge transport properties in the disordered regions. The x-ray-diffraction studies of Fig. 1 show that these materials are structurally inhomogeneous. The model of disorder required to describe the charge transport depends upon the relative values of the temperature-dependent charge delocalization length and of the temperature-independent structural coherence lengths. Low-temperature measurements of the microwave dielectric constant show that the charge delocalization length is the same as the structural coherence length of the ''crystalline'' regions for all samples studied here. In contrast, at ambient temperatures the charge delocalization length is approximately one order of magnitude larger (compare Tables I and IV) than the structural coherence length. Therefore, at ambient temperatures the delocalization length encompasses several ''crystalline'' re-

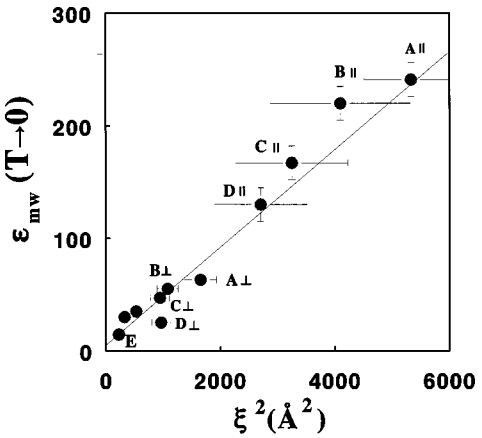

FIG. 11. Plot of $\epsilon_{\mathrm{mw}}(T\rightarrow 0)$ vs the square of crystalline coherence ξ^2 for various XPAN-ES and PAN-ES samples. The $\xi_{\perp}^2$ is assumed to be $\xi_{\perp}^a \times \xi_{\perp}^b$ (from Ref. 25). Note that the lowest value of the three points labeled E corresponds to unstretched material (from Ref. 25), while the next two higher points correspond to the 12.5 times stretched sample E in the perpendicular and parallel directions, respectively.

gions. Hence the role of inhomogeniety is central to the behavior of these materials.

The low-temperature microwave dielectric response of various crystalline polyaniline materials provides information about the intrinsic properties of the metallic (''crystalline'') regions. At low temperatures, the microwave dielectric constant of each sample asymptotically approaches a unique value $\epsilon_{\mathrm{mw}}(T\rightarrow 0)$, which increases with increasing ξ (Fig. 5). Using Eq. (5) in the MBM and assuming $L\sim\xi$, the plot of $\epsilon_{\mathrm{mw}}(T\rightarrow 0)$ vs ξ^2 as shown in Fig. 11 yields the density of states $N(E_F)\sim$ 1.23 states (eV two rings)$^{-1}$. This value is close to that obtained from this and earlier magnetic studies.[35,64] *The fact that* $\epsilon_{\parallel}\propto\xi_{\parallel}^2$ *and* $\epsilon_{\perp}\propto\xi_{\perp}^2$ *with the same proportionality constant demonstrates the 3D nature of the metallic state in the crystalline regions of XPAN-ES systems.* That $\xi\sim L$ shows that the metallic island size is directly related to the crystalline domain length as temperature approaches zero. This is in marked contrast to the small ϵ_{mw} reported[15,29] for the poly(*o*-toluidine) HCl-doped system (POT-HCl) despite its apparent crystalline coherence lengths similar to those of PAN-ES. However, the structural data[65] demonstrate that there is substantial paracrystalline disorder within the POT-HCl ''crystalline'' regimes (due to two possible positions for the substituent methyl group), substantially reducing the coherence of the interchain interaction and hence substantially reducing conduction electron delocalization.

A positive $d\sigma/dT$ and positive dielectric constants in the PAN-HCl and XPAN-HCl samples imply the presence of localization effects in these systems, similar to the behavior of amorphous semiconductors.[17] However, conducting polymers have a very different structural unit, i.e., 1D polymer chains, as compared to 3D bonding of amorphous semiconductors. When polymer chains are coherently aligned, metallic bundles are formed, and the electronic wave functions are three dimensionally delocalized in these metallic bundles. In these regions, one can expect 3D metallic response as for traditional metals. From our study of charge transport as a function of crystallinity in polyaniline materials, the disordered regions between the metallic islands play an important role in the charge localization as ''bottlenecks.'' It is well known that in a metallic chain the localization of carriers arises even for weak disorder because of quantum interference of static scattering.[17] In contrast, if the disordered regions behaved as 3D homogeneously disordered materials, the Ioffe-Regel criterion[66] would require a degree of disorder such that the mean free path is comparable with the Fermi wavelength, i.e., small transport time. For standard metals, this criterion corresponds to very strong disorder and hence very low σ_{dc} at room temperature. This mechanism is unlikely for the chain-structured conducting polymers.

The data presented here support that the localization effects in the inhomogeneously disordered conducting polymers originate from the 1D disordered chains in the disordered regions. A detailed description for 1D localization effects was presented in Ref. 19. If the degree of order in the disordered regions increases (representing the existence of more ordered (larger radius of curvature) chains between the metallic regions) the hopping contribution to the charge transfer within the disordered regions with an active interchain interaction is dominant as compared to direct tunneling between the metallic regions. The results of the high-electric-field-dependent conductivity of sample B (i.e., $\sigma(E)=\sigma_0\exp[(E/E_0)^{1/2}]$) and the existence of the anisotropy of $\sigma_{\mathrm{dc}}(\|)/\sigma_{\mathrm{dc}}(\perp)$ and $\epsilon_{\mathrm{mw}}(\|)/\epsilon_{\mathrm{mw}}(\perp)$ support the applicability of the quasi-1D VRH model. It is pointed out that some samples of PAN show nearly no spatial correlations in the disordered regions,[67] leading to very short localization lengths. This may account for the possible dominance of direct charging energy limited tunneling between the ordered regions[33] in some samples.

The nearly exponential increase of the microwave dielectric constant as temperature increases is accounted for by the model of Ref. 46, which emphasizes the importance of quasi-1D interchain interaction in anisotropic systems. The value of T_0 based on the quasi-1D VRH model becomes small, and the temperature dependence of the thermoelectric power becomes metallic as the order increases. This supports that the polymer chains in the disordered regions are more aligned and contribute to the charge delocalization between the metallic islands.

The exponential increase of ϵ_{mw} with temperature for the more crystalline samples A–C indicates that the charge can be easily delocalized through well-ordered polymer chains. The range of charge localization is no longer microscopic for those materials. The effective delocalization length L_{eff}(RT) using the room-temperature dielectric constant and the MBM model is estimated assuming that $N(E_F)$ is independent of temperature (Table IV). $L_{\mathrm{eff}}(RT)$ *on the order of* $\sim 10^3$ *Å represents a mesoscopic scale for charge delocalization.* The volume V_c of the crystalline region is estimated as $\sim 1.3\times 10^5$ Å^3 utilizing $\xi_{\parallel}$, $\xi_{\perp}^a$, and $\xi_{\perp}^b$ in Table I. Using the 50% crystallinity of sample A obtained from x-ray-diffraction experiments, the volume per crystallite surrounded by its disordered ''shell'' is approximately $V_t=2V_c\sim 2.6\times 10^5$ Å^3. The volume V_d of delocalization at room temperature can also be calculated as $\sim 1.6\times 10^8$ Å^3 using $L_{\parallel,\mathrm{eff}}$(RT) and $L_{\perp,\mathrm{eff}}$(RT). The ratio $\sqrt[3]{V_d/V_t}$ is ~ 8, which implies that charge delocalization extends over ~ 8 metallic islands in any direction assuming isotropic delocalization. Similar con-

clusions are obtained for samples B and C. However, for samples D and E, T_0 is relatively large compared to samples A–C, indicating increased disorder for the polymer chains connecting metallic regions, and the metallic island size is smaller than that of samples A–C [i.e., the values of $\epsilon_{\mathrm{mw}}(T\rightarrow 0)$ and ξ in samples D and E are smaller]. For sample D, the crystallinity is $\sim$30% and $V_c \simeq 6.2\times 10^4$ Å^3. The total volume of an average crystallite and its associated disordered region ($V_t = V_c/0.3$) is $\sim 2.1\times 10^5$ Å^3, and the delocalization volume obtained is $\sim 4.3\times 10^6$ Å^3 using L_{eff}(RT). The ratio $\sqrt[3]{V_d/V_t}$ is smaller than three metallic islands. This indicates that charges remain within the vicinity of one or two metallic islands due to the relatively small size of the metallic islands and the presence of greater disorder in the disordered regions. The models for the anomalous sample and temperature-dependent thermopower and EPR susceptibility and linewidths agree with the model.

VI. SUMMARY

Physically cross-linked HCl-doped polyaniline systems are shown to be inhomogeneously disordered with charge delocalization of the doped polyaniline structurally controlled by chemical processing. The three-dimensional ''metallic islands'' (associated at low temperatures with crystalline regions) are connected through the disordered polymer chains. The linear dependence of $\epsilon_{\mathrm{mw}}(T\rightarrow 0)$ on ξ^2 in both parallel and perpendicular directions shows that the metallic state of crystalline regions in polyaniline has a 3D nature, and demonstrates the generality of the results for the various crystalline samples. As the size of the crystalline regions increases and the chains in the disordered regions are more aligned, the conductivity and microwave dielectric constant increase, and the temperature dependence of the thermoelectric power approaches a nearly metallic behavior. Similarly, the delocalized electrons affect the EPR linewidth through a conduction-electron-localized polaron relaxation mechanism. The very large positive ϵ_{mw} of the highest crystalline materials at room temperature is interpreted as the response of a mesoscopic metallic state due to the relatively large effective size of the ''metallic islands'' and the relatively easy charge transfer through the well ordered chains in disordered regions. The model of Ref. 46 was applied to account for the exponential temperature dependence of ϵ_{mw} for the highest crystalline materials at high temperatures. The quasi-1D VRH model, emphasizing a nearest-neighbor chain hopping, was used to account for the charge transport mechanism in the disordered regions. Furthur improvements in structural order would then lead to full delocalization of a (processing dependent) fraction of conduction electrons.

ACKNOWLEDGMENTS

The authors thank V. N. Prigodin for useful discussions, G. Du, Y. Min, and Z. Oblakowski for cooperation with experiments, and K. R. Brenneman for assistance. This work was supported in part by the Office of Naval Research and Advanced Materials Chemistry Research Center in Korea University (Korea Research Foundation, 96-05-D-1134).

*Permanent address: Department of Chemistry, Myong-Ji University, Kyungkee-Do, Korea.

[1] C. K. Chaing, C. R. Fincher, Jr., Y. W. Park, A. J. Heeger, H. Shirakawa, E. J. Louis, S. C. Gau, and A. G. MacDiarmid, Phys. Rev. Lett. **39**, 1098 (1977).

[2] For examples of recent work, see Proceedings of the International Conference on the Science and Technology of Synthetic Metals, Snowbird, 1996 [Synth. Met. **84–86**, 1–2454 (1997)]; Proceedings of the International Conference on the Science and Technology of Synthetic Metals, Seoul, Korea, 1994 [*ibid.* **69–71**, 1–2320 (1995)]; Proceedings of the International Conference on the Science and Technology of Synthetic Metals, Goteberg, Sweden, 1992 [*ibid.* **55–57**, 1–5124 (1993)]; Proceedings of the Workshop on the Metal Phase of Condensed Polymers [*ibid.* **65**, 89–268 (1994)]; R. S. Kohlman, J. Joo, and A. J. Epstein, *Handbook of the Physical Properties of Polymers*, edited by J. E. Mark (AIP, New York, 1996); J. W. Blatchford and A. J. Epstein, Am. J. Phys. **64**, 120 (1996).

[3] W. P. Su, J. R. Schrieffer, and A. J. Heeger, Phys. Rev. Lett. **42**, 1698 (1979); A. J. Heeger, S. A. Kivelson, J. R. Schrieffer, and W. P. Su, Rev. Mod. Phys. **60**, 781 (1988); M. J. Rice, Phys. Lett. **71A**, 152 (1979); S. A. Brazovskii, Pis'ma Zh. Eksp. Teor. Fiz. **28**, 656 (1978) [JETP Lett. **28**, 606 (1979)]; S. A. Brazovskii and N. N. Kirova, *ibid.* **33**, 6 (1981) [*ibid.* **33**, 4 (1981)].

[4] S. Kivelson, Phys. Rev. Lett. **46**, 1344 (1981); Phys. Rev. B **25**, 3798 (1982).

[5] M. Nechtschein, F. Devreux, R. L. Greene, T. C. Clarke, and G. B. Street, Phys. Rev. Lett. **44**, 356 (1980).

[6] F. Zuo, M. Angelopoulos, A. G. MacDiarmid, and A. J. Epstein, Phys. Rev. B **39**, 3570 (1989).

[7] H. H. S. Javadi, K. R. Cromack, A. G. MacDiarmid, and A. J. Epstein, Phys. Rev. B **39**, 3579 (1989).

[8] A. J. Epstein, H. Rommelmann, M. Abkowitz, and H. W. Gibson, Phys. Rev. Lett. **47**, 1549 (1981).

[9] H. W. Gibson, F. C. Bailey, A. J. Epstein, H. Rommelmann, S. Kaplan, J. Harbour, X.-Q. Yang, D. B. Tanner, and J. M. Pochan, J. Am. Chem. Soc. **105**, 4417 (1983).

[10] L. Zuppiroli, M. N. Bussac, S. Paschen, O. Chauvet, and L. Forro, Phys. Rev. B **50**, 5196 (1994).

[11] R. Pelster, G. Nimtz, and B. Wessling, Phys. Rev. B **49**, 12 718 (1994).

[12] R. Menon, C. O. Yoon, D. Moses, and A. J. Heeger, in *Handbook of Organic Conductive Molecules and Polymers*, edited by H. S. Nalwa (Wiley, New York, 1996).

[13] N. J. Pinto, P. K. Kahol, B. J. McCormick, N. S. Dalal, and H. Wan, Phys. Rev. B **49**, 13 983 (1994).

[14] J. Tsukamoto, Adv. Phys. **41**, 509 (1992).

[15] Z. H. Wang, C. Li, E. M. Scherr, A. G. MacDiarmid, and A. J. Epstein, Phys. Rev. Lett. **66**, 1745 (1991).

[16] A. J. Epstein, H. Rommelmann, R. Bigelow, H. W. Gibson, D. M. Hoffman, and D. B. Tanner, Phys. Rev. Lett. **50**, 1866 (1983).

[17] N. F. Mott and E. Davis, *Electronic Processes in Non-Crystalline Materials* (Clarendon, Oxford, 1979), and references therein.

[18] V. N. Prigodin and K. B. Efetov, Phys. Rev. Lett. **70**, 2932 (1993).

[19] J. Joo, V. N. Prigodin, Y. G. Min, A. G. MacDiarmid, and A. J. Epstein, Phys. Rev. B **50**, 12 226 (1994).

[20] R. S. Kohlman, J. Joo, Y. Z. Wang, J. P. Pouget, H. Kaneko, T. Ishiguro, and A. J. Epstein, Phys. Rev. Lett. **74**, 773 (1995).

[21] Z. H. Wang, A. Ray, A. G. MacDiarmid, and A. J. Epstein, Phys. Rev. B **43**, 4373 (1991).
[22] R. S. Kohlman, J. Joo, Y. G. Min, A. G. MacDiarmid, and A. J. Epstein, Phys. Rev. Lett. **77**, 2766 (1996).
[23] R. S. Kohlman and A. J. Epstein, in *Handbook of Conducting Polymers*, 2nd ed., edited by T. Skotheim *et al.* (Dekker, New York, 1997), Chap. 3, p. 85.
[24] P. Phillips and H.-L. Wu, Science **252**, 1805 (1991); H-L. Wu and P. Phillips, Phys. Rev. Lett. **66**, 1366 (1991).
[25] J. Joo, Z. Oblakowski, G. Du, J. P. Pouget, E. J. Oh, J. M. Wiesinger, Y. Min, A. G. MacDiarmid, and A. J. Epstein, Phys. Rev. B **49**, 2977 (1994).
[26] M. I. Salkola and S. A. Kivelson, Phys. Rev. B **50**, 13 962 (1994).
[27] S. Stafström, Phys. Rev. B **47**, 12 437 (1993).
[28] E. M. Conwell and H. A. Mizes, Synth. Met. **65**, 203 (1994).
[29] Z. H. Wang, E. M. Scherr, A. G. MacDiarmid, and A. J. Epstein, Phys. Rev. B **45**, 4190 (1992).
[30] A. J. Epstein, J. Joo, R. S. Kohlman, G. Du, A. G. MacDiarmid, E. J. Oh, Y. Min, J. Tsukamoto, H. Kaneko, and J. P. Pouget, Synth. Met. **65**, 149 (1994).
[31] M. Reghu, C. O. Yoon, D. Moses, A. J. Heeger, and Y. Cao, Phys. Rev. B **48**, 17 685 (1993); K. Väkiparta, M. Reghu, M. R. Andersson, Y. Cao, D. Moses, and A. J. Heeger, *ibid.* **47**, 9977 (1993).
[32] P. Sheng, B. Abeles, and Y. Arie, Phys. Rev. Lett. **31**, 44 (1973); Q. Li, L. Cruz, and P. Phillips, Phys. Rev. B **47**, 1840 (1993).
[33] F. Zuo, M. Angelopoulos, A. G. MacDiarmid, and A. J. Epstein, Phys. Rev. B **36**, 3475 (1987).
[34] J.-C. Chiang and A. G. MacDiarmid, Synth. Met. **13**, 193 (1986).
[35] A. J. Epstein, J. M. Ginder, F. Zuo, R. W. Bigelow, H.-S. Woo, D. B. Tanner, A. F. Richter, W.-S. Huang, and A. G. MacDiarmid, Synth. Met. **18**, 303 (1987).
[36] H. H. S. Javadi, K. R. Cromack, A. G. MacDiarmid, and A. J. Epstein, Phys. Rev. B **39**, 3579 (1989).
[37] N. J. Pinto, P. K. Kahol, B. J. McCormick, N. S. Dalal, and H. Wan, Phys. Rev. B **49**, 13 983 (1994); P. K. Kahol, and B. J. McCormick, *ibid.* **47**, 14 588 (1993); P. K. Kahol, H. Guan, and B. J. McCormick, *ibid.* **44**, 10 393 (1991).
[38] A. G. MacDiarmid, Y. Min, J. M. Wiesinger, E. J. Oh, E. M. Scherr, and A. J. Epstein, Synth. Met. **55**, 753 (1993).
[39] Y. Cao, P. Smith, and A. J. Heeger, Synth. Met. **48**, 91 (1992).
[40] A. G. MacDiarmid and A. J. Epstein, Synth. Met. **65**, 103 (1994).
[41] I. Webman, J. Jortner, and M. H. Cohen, Phys. Rev. B **16**, 2959 (1977).
[42] O. Levy and D. J. Bergman, J. Phys. A **25**, 1875 (1992).
[43] M. E. Jozefowicz, R. Laversanne, H. H. S. Javadi, A. J. Epstein, J. P. Pouget, X. Tang, and A. G. MacDiarmid, Phys. Rev. B **39**, 12 958 (1989).
[44] M. Cini and P. Ascarell, J. Phys. F **4**, 1998 (1974).
[45] M. J. Rice and J. Bernasconi, J. Phys. F **2**, 905 (1972).
[46] E. P. Nakhmedov, V. N. Prigodin, and A. N. Samukhin, Fiz. Tverd. Tela. (Leningrad) **31**, 31 (1989) [Sov. Phys. Solid State **31**, 386 (1989)].
[47] A. Guinier, *X-Ray Diffraction in Crystals, Imperfect Crystals and Amorphous Bodies* (Dover, New York, 1994).
[48] P. M. Chaikin and J. F. Kwak, Rev. Sci. Instrum. **46**, 218 (1975).
[49] L. Buravov and I. F. Shchegolev, Prib. Tekh. Eksp. **2**, 171 (1971) [Instrum. Exp. Tech. **14**, 528 (1971)].
[50] J. Joo and A. J. Epstein, Rev. Sci. Instrum. **65**, 2653 (1994).
[51] We correct the misprint on p. 4196 of Ref. 29. $\Delta=(F-F_0)/F_0$ should read $\Delta=(F-F_0)/f_0$ where f_0 is the resonance frequency of the empty cavity and $F(F_0)$ is the resonance full width at half maximum with (without) a sample in the cavity.
[52] The samples were folded and gently crushed into irregular-shaped balls, and therefore the EPR line shapes contains both parallel and perpendicular orientation.
[53] K. R. Cromack, J. M. Ginder, M. E. Jozefowicz, R. P. McCall, G. Du, K. Kim, C. Li, Z. Wang, A. J. Epstein, E. M. Scherr, and A. G. MacDiarmid, Macromolecules **24**, 4157 (1991).
[54] J. P. Pouget, M. E. Jozefowicz, A. J. Epstein, X. Tang, and A. G. MacDiarmid, Macromolecules **24**, 779 (1991).
[55] J. P. Pouget, Z. Oblakowski, Y. Nogami, P. A. Albouy, M. Laridjani, E. J. Oh, Y. Min, A. G. MacDiarmid, J. Tsukamoto, T. Ishiguro, and A. J. Epstein, Synth. Met. **65**, 131 (1994).
[56] J. P. Pouget, A. J. Epstein, and A. G. MacDiarmid (unpublished). X-ray-diffraction studies of doped portions of the same undoped high-MW XPAN films from which segments were used to stretch to form samples A and B.
[57] J. P. Pouget, A. J. Epstein, and A. G. MacDiarmid (unpublished). X-ray-diffraction studies of doped portions of the same undoped low-MW XPAN films from which segments were used to stretch to form sample C.
[58] J. E. Wertz and J. R. Bolton, *Electron Spin Resonance: Elementary Theory and Practical Applications* (McGraw-Hill, New York, 1964).
[59] B. R. Weinberger, E. Ehrenfreund, A. Pron, A. J. Heeger, and A. G. MacDiarmid, J. Chem. Phys. **72**, 4749 (1980).
[60] Z. H. Wang, A. Ray, A. G. MacDiarmid, and A. J. Epstein, Phys. Rev. B **43**, 4373 (1991).
[61] H. H. S. Javadi, R. Laversanne, A. J. Epstein, R. K. Kohli, E. M. Scherr, and A. G. MacDiarmid, Synth. Met. **29**, E439 (1989).
[62] H. Hasegawa, Prog. Theor. Phys. **21**, 483 (1959).
[63] S. E. Barnes, Adv. Phys. **30**, 801 (1981).
[64] J. M. Ginder, A. F. Richter, A. G. MacDiarmid, and A. J. Epstein, Solid State Commun. **63**, 97 (1987).
[65] M. E. Jozefowicz, A. J. Epstein, J. P. Pouget, J. G. Masters, A. Ray, and A. G. MacDiarmid, Macromolecules **24**, 5863 (1991); Y. Z. Wang, J. Joo, C.-H. Hsu, J. P. Pouget, and A. J. Epstein, Phys. Rev. B **50**, 16 811 (1994).
[66] A. F. Ioffe and A. R. Regel, Prog. Semicond. **4**, 237 (1960).
[67] M. Laridjani, J. P. Pouget, A. G. MacDiarmid, and A. J. Epstein (unpublished).